

SMECTIC-LIKE PHASE FOR MODULATED XY SPINS IN TWO DIMENSIONS

February 5, 2020

M. Gabay

Laboratoire de Physique des Solides Laboratoire associé au CNRS, Université de
Paris-Sud,
Bâtiment 510, 91405 Orsay Cedex, France

M. Benakli

Department of Physics, Condensed Matter Section, ICTP, P.O. Box 586, 34014
Trieste, Italy

and W.M. Saslow

Department of Physics, Texas A&M University, College Station, Texas 77843-4242

Abstract

The row model for frustrated XY spins on a triangular lattice in 2D is used to study incommensurate (IC) and commensurate (C) phases, in the regime where a (C)-(IC) transition may be observed. Thermodynamic quantities for the (IC) state are computed analytically by means of the NSCHA, a new variational method appropriate for frustrated systems. On the commensurate side of the (C)-(IC) boundary, NSCHA predicts an instability of the (C) phase suggesting that this state is in fact spatially inhomogeneous. Detailed Monte-Carlo (MC) simulations using fluctuating boundary conditions and specific histogram techniques show that in this regime the configuration consists of stripes of (C) and (IC) phases alternating in space. This state, which resembles the smectic-A phase of liquid crystals, exists because of the strong coupling between chiral and phase (spin angle) variables. As a result, the transition between the (IC) and the (C) states can only occur at zero temperature T so that the Lifshitz point is at $T = 0$ for modulated XY spins in 2D.

PACS Number 75.10.Hk

I. INTRODUCTION

Frustration is an ubiquitous phenomenon in condensed matter physics. It occurs whenever several ground states of a system compete at different length scales. Examples of such a situation are non-interacting electrons in a tight binding potential subjected to a uniform magnetic field¹, networks of superconducting wires² or of Josephson junctions³ in a field and spins with competing interactions⁴. In particular, frustrated magnetic systems have been used in the quantum case as realizations of the spin liquid state⁵ (advocated in the context of high T_c superconductors) and in the classical case as representations of the vortex state of layered, strong type II superconductors⁶. Hereafter we consider classical XY ($O(2)$) spins; frustration leads to an additional Z_2 chiral symmetry, so that two scenarios can be considered to describe the critical behavior of these systems: either the Z_2 and the $O(2)$ symmetries are broken at different temperatures, yielding two distinct phase transitions or they are broken at the same temperature, giving a single critical point. Despite extensive analytical and numerical work, this issue still remains unsettled for two dimensional (D=2) XY spin systems^{7–10}. In an attempt to solve the problem, some authors have introduced symmetry breaking fields¹¹: these fields tune the temperature of the Kosterlitz-Thouless (KT) transition¹² (for the $O(2)$ part) and of the Ising transition (for the chiral part).

In particular the row model is a generalization of the fully frustrated XY model on the triangular lattice (FFTXY) where all the bonds strengths J are multiplied by η in the horizontal direction^{13–15}. The FFTXY model corresponds to $\eta = 1$. At $T = 0$, one gets a collinear antiferromagnetic phase (C) for $\eta < 0.5$; this state has

no chirality and only the $O(2)$ symmetry is broken. For $\eta > 0.5$ an incommensurate spiral phase (IC) is obtained; in this regime the two chiral groundstates correspond to the two possible handedness of the spiral and both the $O(2)$ and the Z_2 symmetries are broken. A second order (C)-(IC) transition occurs for $\eta = 0.5$.

Increasing the temperature causes the system ultimately to reach the paramagnetic (P) boundary. For $\eta > 0.5$ this can occur in one or two stages, as discussed above. In the case $\eta < 0.5$ one simply expects a KT transition.

A MC algorithm with "self determined (Fluctuating) Boundary Conditions" (FBC) was developed to study this¹⁶ and other (IC) structures¹⁷. The resulting η versus T phase diagram showed the existence of a continuous (C)-(IC) transition line starting at $\eta = 0.5$ for $T = 0$ and ending at a Lifshitz point¹⁸ (LP) for $\eta_L \simeq 0.62$ and $T_L \simeq 0.42J$. This result raises several issues:

- For 2D modulated $O(N)$ spin systems, renormalization group analysis predicts¹⁹ that the LP is at $T = 0$ whenever $N > 2$; moreover, numerical studies show that this also holds if $N = 1$ (ANNNI model)²⁰. One might have then expected a zero temperature LP for $N = 2$: using a phase-only Hamiltonian, Garel and Doniach indeed reached this conclusion for the so-called $J_1 - J_2$ model²¹.
- According to previous MC simulations¹⁶, increasing T at fixed η ($0.5 < \eta < \eta_L$) produced the following sequence of phases: an (IC) state is observed at low T ; then, across the (C)-(IC) transition, at T_{C-IC} , one moves into the (C) phase; lastly one reaches the (P) boundary at T_P . In this process one of the eigenvalues of the spinwave stiffness matrix decreases uniformly as T varies

from zero to T_{C-IC} , vanishes at T_{C-IC} , increases again in the (C) phase and becomes zero above T_P . However for $T \geq T_{C-IC}$ one may analytically compute the bare (unrenormalized) stiffness constant; one finds that it is very small. In this regime, the KT renormalization group equations^{12,22} would predict that vortex-antivortex pairs are unbound, implying that the (C) phase is thermodynamically unstable near the (C)-(IC) transition. This result suggests a reentrant (P) phase and thus a zero temperature Lifshitz point in agreement with Garel and Doniach but at variance with Monte Carlo results.

The present paper shows how these a-priori conflicting conclusions can be reconciled:

In section II, using the NSCHA method (New Self-consistent Harmonic Approximation), a recently developed variational approach for frustrated systems⁸, we study the (IC) phase and the approach to the (C)-(IC) transition. We find that, for $T \rightarrow T_{C-IC}^{(-)}$, the eigenvalue γ^{xx} of the spin wave stiffness matrix associated with the incommensurate direction goes to zero, but the corresponding wavevector, Q_x , remains strongly incommensurate near T_{C-IC} . The other eigenvalue γ^{yy} remains finite at T_{C-IC} . For $T > T_{C-IC}$ a (C) solution is obtained but $\gamma^{xx} < 0$, so that the (C) phase is thermodynamically unstable. Thermal fluctuations for $T \leq T_{C-IC}$ as well as for $T \geq T_{C-IC}$ are characterized by a coupling between phase (spin angles) and chiral degrees of freedom. Within NSCHA the coupling is thus relevant at all T . The instability of the (C) phase for $T \geq T_{C-IC}$ is interpreted as indicating a spatially inhomogeneous state where chiral and collinear domains coexist. This state is inaccessible to our variational scheme which assumes homogeneous solutions.

In section III, we present the MC methodology required to study incommen-

surate and spatially inhomogeneous states. In the presence of domains, local and global variables do not yield identical thermodynamic results. We show how to extract relevant quantities from a MC algorithm using FBC and specific histogram techniques designed for FBC. This approach allows us to analyse the data near the (C)-(IC) transition. Section IV is a MC study of the row model for fixed η , with $0.5 < \eta < \eta_L$, at various T . Special attention is devoted to the "(C) phase" for $T \geq T_{C-IC}$. Fig (12) shows a striped structure confirming that domains of opposite chirality separated by walls of the collinear phase coexist. Such a spatially inhomogeneous state resembles the smectic-A phase of liquid crystals. In this regime (Fig (13)) $\gamma^{xx} = 0$ and $\gamma^{yy} > 0$. Stripes exist because the coupling between phase and chiral variables is relevant at all T when $\eta > 0.5$. This coupling helps explain why domains of the chiral phase are present for $T \geq T_{C-IC}$. Moreover, fluctuations between a spatially homogenous state (the incommensurate phase) and a spatially inhomogeneous spiral domain state (the striped phase) do not allow simple scaling analysis of critical quantities at T_{C-IC} (Fig (14)).

These observations indicate that the (C) and (IC) phases are connected by a smectic-like state, and only come in contact at $T = 0$ and $\eta = 0.5$, so that the LP is indeed at $T = 0$ for the 2D XY model. On the other hand there is no re-entrant (P) phase between the (C) and (IC) regions.

II. NSCHA FOR THE COMMENSURATE AND INCOMMENSURATE REGIMES

In a previous paper we introduced the new self-consistent harmonic approximation (NSCHA)⁸, a variational technique appropriate for frustrated systems. The main feature of this approach is that it preserves the coupling between the chiral ground states of the system, and that it takes long wavelength chiral fluctuations into account. Chiral and phase (spin angle) variables remain coupled at all temperature T. We begin by recalling the basics steps of the method and we next apply it to the row model.

A. The NSCHA variational method.

The Hamiltonian for XY spins characterized by spin angles $\{\theta_i\}$, reads

$$H = - \sum_{\langle ij \rangle} J_{ij} \cos(\theta_i - \theta_j) \quad (1)$$

where the J_{ij} are nearest neighbor interactions. For frustrated systems the sign of the product of the J_{ij} over the links of a plaquette P is negative and this may lead to non-collinear configurations in thermal equilibrium. The variational method seeks to approximate H (Eq.1) by an harmonic Hamiltonian H_0 . We rewrite the θ_i in Eq.1 as

$$\theta_i = \theta_i^0 + \varphi_i \quad (2)$$

with $\theta_i^0 = \langle \theta_i \rangle_{H_0}$ and

$$H_0 = \frac{1}{2} \sum_{\langle ij \rangle} \tilde{J}_{ij} (\varphi_i - \varphi_j)^2 \quad (3)$$

Inserting Eq.2 into Eq.1 gives

$$H = - \sum_{\langle ij \rangle} J_{ij} \left[\cos(\theta_i^0 - \theta_j^0) \cos(\varphi_i - \varphi_j) - \sin(\theta_i^0 - \theta_j^0) \sin(\varphi_i - \varphi_j) \right] \quad (4)$$

Averaging H over the variational Hamiltonian H_0 , the $\sin(\dots)$ term in Eq.4 drops out. Since this term discriminates between the two chiral states of the frustrated system, chiral fluctuations are thus eliminated. In the standard variational method H_0 is treated as an effective ferromagnetic Hamiltonian with couplings $J_{ij} \cos(\theta_i^0 - \theta_j^0)$. In contrast, the NSCHA approach preserves the coupling between chiral states and maps Eq.4 onto an effective Hamiltonian:

$$H_{NSCHA} = - \sum_{\langle ij \rangle} J_{ij} \cos(\theta_i^0 - \theta_j^0) \cos(\varphi_i - \varphi_j) - \frac{1}{2T} \sum_{\langle ij \rangle} \sum_{\langle kl \rangle} J_{ij} J_{kl} \times \sin(\theta_i^0 - \theta_j^0) \sin(\theta_k^0 - \theta_l^0) \sin(\varphi_i - \varphi_j) \sin(\varphi_k - \varphi_l) \quad (5)$$

Averaging Eq.5 over H_0 (Eq.3) and minimizing with respect to the variational parameters⁸ θ_i^0 and y_{ij} yields the NSCHA variational equations

$$\begin{aligned} \tilde{J}_{ij} = & J_{ij} \cos(\theta_i^0 - \theta_j^0) e^{-\frac{1}{2}y_{ij}} \\ & + \frac{1}{2T} \sum_{k,l} J_{ij} J_{kl} \sin(\theta_i^0 - \theta_j^0) \sin(\theta_k^0 - \theta_l^0) e^{-\frac{1}{2}(y_{ij} + y_{kl} + y_{ik} + y_{jl} - y_{il} - y_{jk})} \\ & + \frac{1}{T} \sum_{k,l} J_{ik} J_{jl} \sin(\theta_i^0 - \theta_k^0) \sin(\theta_j^0 - \theta_l^0) \\ & \cosh(y_{ij} + y_{kl} - y_{il} - y_{jk}) e^{-\frac{1}{2}(y_{ik} + y_{jl})} \end{aligned} \quad (6)$$

$$\begin{aligned} & \sum_j J_{ij} \sin(\theta_i^0 - \theta_j^0) e^{-\frac{1}{2}y_{ij}} \\ - \frac{1}{2T} \sum_{j,k,l} J_{ij} J_{kl} & \cos(\theta_i^0 - \theta_j^0) \sin(\theta_k^0 - \theta_l^0) e^{-\frac{1}{2}(y_{ij} + y_{kl} + y_{ik} + y_{jl} - y_{il} - y_{jk})} = 0 \end{aligned} \quad (7)$$

with

$$\begin{aligned} y_{ij} &= \left\langle (\varphi_i - \varphi_j)^2 \right\rangle_{H_0} \\ &= \frac{T}{2\pi^2} \int \int_{BZ} d^2 q \frac{1 - \cos(\vec{q} \cdot (\vec{r}_i - \vec{r}_j))}{\tilde{J}(\vec{0}) - \tilde{J}(\vec{q})} \end{aligned} \quad (8)$$

where $\tilde{J}(\vec{q})$ is the Fourier transform of \tilde{J}_{ij} .

In this ensemble we can compute the spinwave stiffness matrix. Its eigenvalues are γ_{NSCHA}^{xx} and γ_{NSCHA}^{yy} :

$$\begin{aligned}\gamma_{NSCHA}^{xx} = & \frac{1}{N} \sum_{\langle ij \rangle} J_{ij} \cos(\theta_i^0 - \theta_j^0) (\vec{u}_{ij} \cdot \vec{u}_x)^2 e^{-y_{ij}/2} \\ & - \frac{1}{N} \frac{1}{T} \sum_{\langle ij \rangle} \sum_{\langle kl \rangle} J_{ij} J_{kl} (\vec{u}_{ij} \cdot \vec{u}_x) (\vec{u}_{kl} \cdot \vec{u}_x) e^{-(y_{ij} + y_{kl} + y_{ik} + y_{jl} - y_{il} - y_{jk})/2} \\ & \times [\cos(\theta_i^0 - \theta_j^0) \cos(\theta_k^0 - \theta_l^0) + \sin(\theta_i^0 - \theta_j^0) \sin(\theta_k^0 - \theta_l^0)]\end{aligned}\quad (9)$$

where \vec{u}_x is the unit vector in the horizontal direction, and \vec{u}_{ij} is the vector connecting nearest neighbor sites i and j . For γ_{NSCHA}^{yy} we replace \vec{u}_x by \vec{u}_y the unit vector in the vertical direction.

We can also compute the staggered chirality:

$$\sigma_{NSCHA} = \frac{1}{N_P} \sum_{\{P\}} \frac{\left\langle \sum_{\langle kl \rangle \in P} \sigma_{kl} \right\rangle_{H_0}}{\sum_{\langle kl \rangle \in P} \sigma_{kl}(T=0)} \quad (10)$$

Here $\sum_{\{P\}}$ denotes summation on plaquettes of the same sublattice, i.e. plaquettes in the same chiral state at $T=0$. The summation $\sum_{\langle kl \rangle \in P}$ is performed over the links of plaquette P oriented clockwise, and σ_{kl} is defined as

$$\sigma_{kl} = J_{kl} \sin(\theta_k - \theta_l) \quad (11)$$

In the NSCHA ensemble one obtains

$$\sigma_{NSCHA} = \frac{\sum_{\langle kl \rangle \in P} J_{kl} \sin(\theta_k^0 - \theta_l^0) e^{-y_{kl}/2}}{\sum_{\langle kl \rangle \in P} J_{kl} \sin(\theta_k^0(T=0) - \theta_l^0(T=0))} \quad (12)$$

B. NSCHA for the row model

The row model is defined on the triangular lattice^{13,14}. Only nearest neighbor sites are coupled: $J_{ij} = -\eta J$ ($J > 0$) for i and j along the horizontal direction and $J_{ij} = -J$ otherwise. In our previous paper we studied the case $\eta = 1$ which corresponds to the FFTXY model. Here we will assume $\eta \neq 1$.

1. Zero temperature limit.

At $T = 0$, Eq.7 yields

$$\theta_i^0 - \theta_j^0 = \vec{Q} \cdot \vec{u}_{ij} \pmod{2\pi} \quad (13)$$

with

$$Q_x = \pm 2\cos^{-1}\left(\frac{1}{2\eta}\right); \quad Q_y = \frac{2\pi}{\sqrt{3}} \pmod{2\pi} \quad (14)$$

or

$$Q_x = 0; \quad Q_y = \frac{2\pi}{\sqrt{3}} \pmod{2\pi} \quad (15)$$

For $\eta \leq 1/2$, Eq.15 gives the collinear ground state, whereas for $\eta > 1/2$ a spiral state is obtained (Eq.14). A second order transition takes place when $\eta = 1/2$.

2. Finite temperature regime.

Eqs.6, 7 and 8 yield two types of solutions:

a) Commensurate solutions:

They are characterized by

$$\theta_i^0 - \theta_j^0 = \vec{Q}^0 \cdot \vec{u}_{ij} \pmod{2\pi} \quad (16)$$

with

$$Q_x^0 = 0; \quad Q_y^0 = \frac{2\pi}{\sqrt{3}} \pmod{2\pi} \quad (17)$$

and by nearest neighbor couplings \tilde{J}_{ij} . There are only two independent interactions namely $\tilde{J}_{ij} = \tilde{\eta} \tilde{J}$ for i and j along the horizontal direction, and $\tilde{J}_{ij} = \tilde{J}$ otherwise. These satisfy the following equations

$$\tilde{J} = J e^{-\frac{T}{\pi \tilde{J}} \tan^{-1}[(1+2\tilde{\eta})^{-1/2}]} \quad (18)$$

$$\tilde{\eta} \tilde{J} = -\eta J e^{-\frac{T}{\pi \tilde{\eta} \tilde{J}} \tan^{-1}[\tilde{\eta}(1+2\tilde{\eta})^{-1/2}]} \quad (19)$$

Eqs.18 and 19 can be self-consistently satisfied without restriction for $\eta \leq 1/2$.

Fig (1) shows γ_{NSCHA}^{xx} and γ_{NSCHA}^{yy} for $\eta = 0.4$: the (C) solution is indeed stable. We note that γ_{NSCHA}^{xx} displays a maximum at some temperature T . This feature was present in the MC simulation of Saslow et al¹⁶. It is the result of the competition between two effects : on the one hand for fixed η , as T increases, one moves farther away from the (C)-(IC) boundary and thus γ_{NSCHA}^{xx} increases; on the other hand thermal fluctuations tend to reduce the value of γ_{NSCHA}^{xx} .

However, if $\eta > 1/2$ equations Eqs.18 and 19 have no solution when $T \leq \frac{J}{\eta} \ln(2\eta)$; this property was expected, since the stable state of the system is a spiral structure at low T , for $\eta > 1/2$.

b) Incommensurate solutions:

They correspond to

$$\theta_i^0 - \theta_j^0 = \vec{Q}^0 \cdot \vec{u}_{ij} \pmod{2\pi} \quad (20)$$

with

$$Q_x^0 = Q_0(T); \quad Q_y^0 = \frac{2\pi}{\sqrt{3}} \pmod{2\pi} \quad (21)$$

In that case Eqs.6, 7 and 8 can only be solved numerically. Just as for the FFTXY model, the \tilde{J}_{ij} are no longer short range interactions and the sign of \tilde{J}_{ij} varies with the relative orientation of i and j . For $\eta = 0.575$, Fig (2) shows $|\tilde{J}(R)|$ versus R ($R = |\vec{r}_i - \vec{r}_j|$) for $T = 0.1J$, and Fig (3) shows the sign of \tilde{J}_{ij} at position $\vec{r}_{ij} = \vec{r}_j - \vec{r}_i$.

At all T we find that the asymptotic behavior of \tilde{J}_{ij} for large R is given by $\tilde{J}_{ij} \sim 1/|\vec{r}_i - \vec{r}_j|^6$ (this can be analytically demonstrated at low T , see Ref.8). This polar-like behavior (power law decay and sign change with the orientation) is a consequence of the coupling between phase and chiral degrees of freedom.

Knowledge of the \tilde{J}_{ij} allows us to compute $Q_0(T)$, γ_{NSCHA}^{xx} , γ_{NSCHA}^{yy} (Eq.9) and σ_{NSCHA} (Eq.12) as a function of T . These quantities are shown on Figs (4), (5), (6) along with the MC data, for $\eta = 0.575$.

The NSCHA and MC results agree closely except in the vicinity of T_{C-IC} , where defects are expected to play an important role (see our previous paper Ref.8).

Beyond T_{C-IC} , one might expect to recover the commensurate solution Eqs.18 and 19. For $\eta = 0.575$, *assuming a second order phase transition*, NSCHA would predict $T_{C-IC} = \ln(2\eta)/\eta \sim 0.24$. However, solving Eqs.6, 7 and 8 gives $T_{C-IC}/J \sim 0.29 > 0.24$. Furthermore $Q_0(T = T_{C-IC}) \neq 0 \pmod{2\pi}$. Also Fig (7) shows the variational free energies for the collinear and for the spiral solutions (see Ref.8, Eq.4): the two branches merge for $T \sim T_{C-IC}$ but their slopes are different.

These findings suggest a first order transition between the (C) and (IC) states. However we find that $\gamma_{NSCHA}^{xx} < 0$ for all $T > T_{C-IC}$: within NSCHA the collinear phase is thermodynamically unstable. The above features revealed by the NSCHA are reminiscent of the thermodynamics of spatially inhomogeneous systems such as dipolar magnets^{23,24}, the vortex state of superconductors, smectic phases²⁵ or spin glasses²⁶. For these systems, one also finds that seeking homogeneous groundstates leads to first order transitions and to the instability of a response function. The instability signals that equilibrium configurations consist of domains separated by domain walls. Accordingly, in our case the commensurate regime would be expected to consist of stripes of the incommensurate phase with opposite chiralities separated by domain walls (non-chiral regions). Locally (that is within a domain) one would have $|Q_x| = Q_0(T_{C-IC}) \neq 0 \pmod{2\pi}$, but averaging over the system size would give $Q_x(T_{C-IC}) = 0 \pmod{2\pi}$. Across the transition, on the low temperature side, a homogeneous spiral state is obtained. We note that, in the domain wall scenario, the transition may be continuous²⁷. This implies in particular that γ^{xx} does not jump discontinuously to zero across T_{C-IC} but rather that it vanishes continuously at $T = T_{C-IC}$ (see Fig (5)). Since our variational approach is based on spatially homogeneous configurations it cannot describe the thermodynamic phase for $T > T_{C-IC}$.

Once again, we emphasize that the instability of the (C) phase is a direct consequence of the chiral fluctuations and of their coupling to phase fluctuations, for all T .

We now turn to the MC study of the row model.

III. MONTE CARLO

A. Fluctuating boundary conditions.

For finite-sized systems, boundaries can lead to undesirable effects resulting from the breaking of translational invariance. In order to remove, or at least to minimize boundary effects, it is customary to choose special conditions at the boundary.

Since the system studied in this paper contains an incommensurate phase, periodic boundary conditions (PBC) are not suitable here. Furthermore, since the pitch of the spiral varies with T and η , these boundary conditions (BC) have to smoothly evolve when one changes external parameters like the anisotropies or the temperature.

Self-consistent boundary conditions, using FBC, have been proposed to overcome these problems^{16,28}. The main feature of FBC is to add new dynamical variables Δ_α ($\alpha = 1, 2, \dots, D$ where D is the dimensionality of the lattice) corresponding to a shift at the boundaries. In equilibrium the new "boundary variables" Δ_α will fluctuate around their *most probable value* Δ_α^0 .

The partition function of an $L \times L$ system of XY spins is:

$$Z = \int \dots \int_{-\pi}^{\pi} \prod_i d\Phi_i e^{-\beta \cdot \left(-\frac{1}{2} \sum_{i,j} J_{ij} \cos(\Phi_i - \Phi_j) \right)} \quad (22)$$

The FBC method amounts to imposing the following constraint at the boundary

$$\Phi(\vec{r} + nL\vec{u}_x + mL\vec{u}_y) = \Phi(\vec{r}) + nL\Delta_x + mL\Delta_y \quad (23)$$

where Δ_x and Δ_y are new *dynamical* degrees of freedom, corresponding to a shift at the boundaries. Note that using FBC allows us to preserve translational invariance (contrary to the free BC). Performing a change of variables

$$\Phi(\vec{r}) = \varphi(\vec{r}) + \vec{\Delta} \cdot \vec{r} \quad (24)$$

with

$$\vec{\Delta} = \Delta_x \vec{u}_x + \Delta_y \vec{u}_y \quad (25)$$

the constraint on φ becomes

$$\varphi(\vec{r} + nL\vec{u}_x + mL\vec{u}_y) = \varphi(\vec{r}) \quad (26)$$

In terms of the new variable φ the partition function of the $L \times L$ system with FBC is:

$$Z_{FBC} = L^2 \int_{-\pi/L}^{\pi/L} d^2 \Delta \left(\int \dots \int_{-\pi}^{\pi} \prod_i d\varphi_i e^{-\beta \cdot \left(-\frac{1}{2} \sum_{i,j} J_{ij} \cos(\varphi_i - \varphi_j - \vec{\Delta} \cdot (\vec{r}_i - \vec{r}_j)) \right)} \right) \quad (27)$$

Wrapping the lattice around a torus automatically enforces the constraint $\varphi(\vec{r} + nL\vec{u}_x + mL\vec{u}_y) = \varphi(\vec{r})$. It is important to note that the integration in Eq.27 is over an interval of size 2π for φ_i , whereas it is over a $2\pi/L$ interval for $\Delta_{x,y}$. The interval of integration corresponds to the periodicity of the Hamiltonian.

Z_{FBC} can be factorized as a product of a set of partition functions, $Z(\vec{\Delta})$, each one corresponding to a fixed shift $\vec{\Delta}$ at the boundaries:

$$Z_{FBC} = L^2 \int_{-\pi/L}^{\pi/L} Z(\vec{\Delta}) d^2 \Delta = L^2 \int_{-\pi/L}^{\pi/L} d^2 \Delta e^{-\beta L^2 f(\vec{\Delta})} \quad (28)$$

where $f(\vec{\Delta})$ is the $\frac{2\pi}{L}$ periodic free energy per spin associated with the shift $\vec{\Delta}$ at the boundary: $f(\vec{\Delta}) = T \ln(Z(\vec{\Delta}))/L^2$. For $\vec{\Delta} = \vec{0}$, we recover the PBC case, i.e. $Z_{PBC} = Z(\vec{\Delta} = \vec{0})$ and $f_{PBC} = f(\vec{\Delta} = \vec{0})$.

For a system with a helical phase at low temperature, $f(\vec{\Delta})$ displays a minimum for $\vec{\Delta} = \vec{\Delta}^0$. $\vec{\Delta}^0$ is determined *modulo* $\frac{2\pi}{L}$ from:

$$\frac{\delta f(\vec{\Delta})}{\delta \Delta_x} \bigg|_{\vec{\Delta}^0} = 0, \quad \frac{\delta f(\vec{\Delta})}{\delta \Delta_y} \bigg|_{\vec{\Delta}^0} = 0 \quad (29)$$

For a spiral phase, the pitch \vec{Q}_0 , is the $\frac{2\pi}{L}$ determination of $\vec{\Delta}_0$ such that $\varphi(\vec{r}) \simeq 0$ in equilibrium (see Eq.24).

Expanding $f(\vec{\Delta})$ to second order in $\vec{\Delta}$ near $\vec{\Delta}^0$ gives

$$f(\vec{\Delta}^0) + \frac{1}{2} \frac{\delta^2 f(\vec{\Delta})}{\delta \Delta_x^2} \bigg|_{\vec{\Delta}^0} (\Delta_x - \Delta_x^0)^2 + \frac{1}{2} \frac{\delta^2 f(\vec{\Delta})}{\delta \Delta_y^2} \bigg|_{\vec{\Delta}^0} (\Delta_y - \Delta_y^0)^2 + O(\Delta^4) \quad (30)$$

The second derivatives of the free energy are related to the components γ^{xx}, γ^{yy} of the spin rigidity²² by a geometrical factor ρ

$$\gamma^{xx} = \rho \frac{\delta^2 f(\vec{\Delta})}{\delta \Delta_x^2} \bigg|_{\vec{\Delta}^0}, \quad \gamma^{yy} = \rho \frac{\delta^2 f(\vec{\Delta})}{\delta \Delta_y^2} \bigg|_{\vec{\Delta}^0} \quad (31)$$

ρ is 1 for the square lattice, and $\frac{2}{\sqrt{3}}$ for the triangular lattice.

At low T and far from the (C)-(IC) boundary (where $\gamma^{xx} = 0$), $\beta\gamma^{xx} \gg 1$ and $\beta\gamma^{yy} \gg 1$. Inserting Eq.30 into Eq.28 using Eq.31 then gives¹⁶

$$\gamma^{xx} = \frac{\rho}{L^2 \chi_{\Delta_x}}, \quad \gamma^{yy} = \frac{\rho}{L^2 \chi_{\Delta_y}} \quad (32)$$

where $\chi_{\Delta_x} = \beta \langle (\Delta_x - \Delta_x^0)^2 \rangle$ (resp. $\chi_{\Delta_y} = \beta \langle (\Delta_y - \Delta_y^0)^2 \rangle$) is the susceptibility for Δ_x (resp. Δ_y).

B. Δ -Histograms

In the previous section we showed that the partition function with FBC is a sum over partition functions $Z(\vec{\Delta})$. A practical way to perform this sum is to count

the number of configurations obtained for each of the allowed values of Δ_x and Δ_y . Since Δ_x and Δ_y are defined modulo $\frac{2\pi}{L}$, this can be easily done by histograms in Δ_x and Δ_y , which we call Δ -histograms.

From the standpoint of a Monte Carlo simulation, histograms are generated as follows: we divide the range of variation of Δ_x and Δ_y into smaller sub-intervals. For each of these we store the total number of configurations $n(\Delta_x, \Delta_y)$ having Δ_x and Δ_y within the given interval, and also the average of relevant quantities (such as the energy, the chiral order parameter) over these configurations.

This yields the probability distribution $P(\Delta_x, \Delta_y)$ for Δ , and averages $O^{hist}(\Delta_x, \Delta_y)$ of various observables.

$P(\Delta_x, \Delta_y)$ is given by

$$P(\Delta_x, \Delta_y) = \frac{n(\Delta_x, \Delta_y)}{\mathcal{N}} \quad (33)$$

where \mathcal{N} is the total number of generated configurations.

The Δ -histogram free energy is obtained from:

$$f(\vec{\Delta}) = -\frac{1}{\beta L^2} \ln(P(\Delta_x, \Delta_y)) + Constant \quad (34)$$

The zeroes of the first derivative of the free energy yield the value of $\vec{\Delta}^0$. The second derivatives of the free energy computed for $\vec{\Delta} = \vec{\Delta}^0$ give the components of the spinwave stiffness γ , by Eq.31. In addition, using histograms can give information about the nature of the commensurate-incommensurate (C)-(IC) transition: in the incommensurate phase, the free energy displays two minima at $\pm \vec{\Delta}_0$. A first order transition will be characterized by the coexistence of a third local minimum in $f(\vec{\Delta})$ for $\vec{\Delta} = \vec{0}$, at some characteristic temperature.

Let us note that for FBC without Δ -histograms¹⁶, γ^{xx} is obtained from the approximate expression Eq.32:

$$\gamma^{xx} \simeq \frac{\rho}{L^2 \chi_{\Delta_x}} \simeq \frac{\rho}{L^2 \chi_{Q_x}} \quad (35)$$

where Q_x is the pitch of the helimagnetic state. The average pitch $(Q_x)_{ave}$ is computed as the average of the pitch of the system over all the generated configurations:

$$(Q_x)_{ave} = \langle Q_x \rangle_{FBC} \quad (36)$$

Similar expressions hold for γ^{yy} and $(Q_y)_{ave}$. This method gives good results if $\beta\gamma^{xx} \gg 1$ and if $\beta\gamma^{yy} \gg 1$; in this limit one should not expect any significant differences from histogram-based approaches. *However, the method fails in the vicinity of the (C)-(IC) line, where $\beta\gamma^{xx} \rightarrow 0$, so that it is not well suited for a scaling analysis.*

IV. NUMERICAL ANALYSIS OF THE ROW MODEL

A. The method

Since the incommensurability is only present in the x direction we used hybrid boundary conditions: PBC in the y direction and FBC in the x direction. A standard Metropolis algorithm was applied to the spin angles and to the boundary shift in the x direction. Lattices sizes ranged from 18^2 to 48^2 and the number of MCS/spin was of order $10^5 - 10^6$. Typically the first 10^4 steps were discarded for equilibration. In contrast to our previous study of this system¹⁶, Δ -histograms were included here. These were used to determine Q_0 as well as the spinwave stiffnesses along x and y . In addition, we monitored

- the staggered chiralities $\Sigma = \langle \sigma \rangle$ with

$$\sigma = \frac{1}{N_P} \sum_{\{P\}} \frac{\sum_{\langle kl \rangle \in P} \sigma_{kl}}{\sum_{\langle kl \rangle \in P} \sigma_{kl}(T=0)} \quad (37)$$

where P refers to plaquettes in the same chiral state at $T = 0$

and

$$\sigma_{kl} = J_{kl} \sin(\theta_k - \theta_l) \quad (38)$$

(see Eq.10)

or

$$\sigma_{kl} = \frac{1}{2\pi}(\theta_k - \theta_l) \quad (39)$$

(for Eq.39, the angular determination of the term in parenthesis is taken in the interval $[-\pi, +\pi]$ (see Ref.8)).

- the chiral susceptibility

$$\chi_\sigma = \frac{1}{T} \langle \sigma^2 - \Sigma^2 \rangle \quad (40)$$

- the Binder order parameter for chiralities

$$g_\sigma = \frac{1}{2} \left[3 - \left(\frac{\langle \sigma^4 \rangle}{\langle \sigma^2 \rangle} \right) \right] \quad (41)$$

B. Order-disorder transitions

Using Monte Carlo simulations for a system of size 36^2 , we first studied the commensurate- paramagnetic and the incommensurate- paramagnetic phase transitions. T was varied at fixed η . The divergence of the chiral susceptibility characterizes the Z_2 transition temperature. At the $O(2)$ transition temperature the spin stiffnesses drops to a small – size dependent – value. Our results for the locations of the (C)-(P) and (IC)-(P) lines in the (η, T) plane (Fig (8) accurately reproduce the results of Saslow et al¹⁶.

LCD is a line separating the (C) phase and the (P) phase. This transition correspond to an $O(2)$ symmetry breaking, and thus is in the KT universality class, *except in the vicinity of the Lifshitz point L*; this transition is characterized by a universal jump of the spin stiffness $\gamma = \sqrt{\gamma_{xx}\gamma_{yy}}$.

LB is a line separating the (IC) phase and the (P) phase. Our simulations show that the Z_2 and $O(2)$ transitions occur simultaneously (*within error-bars*, the divergence of the chiral susceptibility and the jump of the spin stiffness are observed at the same T). This behavior is similar to that obtained for the isotropic FFTXY³⁰

C. Study of the (C)-(IC) line

AL is a line separating the spiral incommensurate phase from the commensurate layered antiferromagnetic (C) phase. It is characterized by a divergence of the chiral susceptibility and by the *continuous vanishing* of the x component of the spin stiffness. The y component of the spin stiffness, on the other hand, does not show any non-analiticity near AL. We now focus on the vicinity of the (C)-(IC) transition.

We fix the value η and vary the temperature. Typically we chose $\eta = 0.575$ and $\eta = 0.55$. Starting from the low temperature phase, we observe that $\gamma_{xx} \rightarrow 0$ and that simultaneously the chiral susceptibility diverges as one approaches AL, Fig (5). This behavior can be understood as follows: Eikmans et al's Coulomb gas analysis of the generalized Villain model³¹, when generalized to the row model, gives³²:

$$\gamma_{xx} \propto \frac{1}{\chi_\sigma} \quad (42)$$

Chiral variables and spin angle variables are coupled in the (IC) phase; thus γ_{xx} can go to zero in a continuous fashion, rather than jump, on crossing AL. Similarly from the same Coulomb gas analysis, one expects that γ_{yy} is well behaved across AL (Fig (5)). Fig (9) show that Q_0 also goes to zero (mod 2π) at T_{C-IC} . At first sight, for $T > T_{C-IC}$ the system appears to be in the commensurate phase, but our study shows that the morphology of the state is not a simple one:

Δ -histograms show a three-peak structure for $T \gtrsim T_{C-IC}$. There is a central peak at $\Delta_x = 0$ and two side peaks centered on T dependent, finite values $\pm\Delta_0$. For sizes 48^2 and for simulations using large enough MCS/spin we notice that the relative weight of the lateral peaks compared to the central peak is roughly one (see Fig (10)).

Following our discussion of section II the previous results do not necessarily signal a first order transition across the (C)-(IC) line; this would be at variance with the results pertaining to γ_{xx} and χ_σ which are more consistent with a second order transition. In fact all these data can be consistently interpreted if one considers the possibility of a thermodynamically inhomogeneous commensurate phase. We

mentioned in the introduction that systems with competing interactions may lead to stripe phase groundstates consisting of ordered domains separated by domain walls^{23,24,33,34}. Our simulations reveal that the commensurate phase of the row model may well be such an example of stripe phases: boundaries between domains of opposite chirality consist of walls of zero chirality, that is of regions of the collinear phase. Chiral domains will have either $Q_x = +Q_0(T)$ or $Q_x = -Q_0(T)$ and collinear domains are characterized by $Q_x = 0$. To support this picture we plot the staggered chirality versus T (Eq.39) and the absolute value of the chiralities versus T (where we replace $\sum_{\langle kl \rangle \in P} \sigma_{kl}$ by $\text{Abs}(\sum_{\langle kl \rangle \in P} \sigma_{kl})$ in Eq.(37)). This gives access to the number of plaquettes with positive, negative and zero chirality one each sublattice (see Ref.8). Fig (11) shows that for $\eta = 0.575$ and $T = 0.4J$, well above the (C)-(IC) transition temperature, (i.e, in what should be the commensurate phase), 25% of the plaquettes have a positive chirality, 25% of the plaquettes have a negative chirality, and 50% of the plaquettes have no chirality. With these weights, averaging Q_x over the system yields $Q_x = 0$. In the stripe phase $\gamma_{xx} = 0$. The morphology of this state is shown in Fig (12), which is a snapshot of the chiralities for $\eta = 0.575$ and $T = 0.4J$. Note that the normal to the direction of the stripes correlates with x (the direction of the η -bonds). To map out the domain of stability of the stripe phase in the (η, T) plane, we keep T fixed and we vary η . Fig (13) shows γ_{xx} versus η for $T = 0.2J$ and $T = 0.4J$; in the region delimited by lines AC ($\eta = 0.5$) and AL we get $\gamma_{xx} = 0$ and one expects a stripe phase there. In other words AL separates an incommensurate phase from an inhomogeneous, non-collinear state.

As a result,

1. in the η, T plane, the transition between the spiral phase and the LAF phase is only seen at point A (that is, at zero temperature). Consequently, the Lifshitz point is at $T = 0$ for the 2D XY model.
2. the existence of the stripe phase suggests that chiral variables and phase variables remain strongly coupled at all T . This may explain why, despite the fact that $\gamma_{xx} = 0$ in the stripe phase, vortices do not unbind (leading to a reentrant paramagnetic phase). The relevance of this coupling had already been emphasized in our study of the fully frustrated case ($\eta = 1$).
3. the existence of the inhomogeneous state affects scaling analyses near the (IC)-stripe phase boundary (line AL): Fig (14) shows the Binder order parameter Eq.(41) as a function of T for $\eta = 0.575$. We do not observe a clear intersection at the critical temperature. A similar feature had been pointed out by Olsson in his study of fully frustrated XY spins on a 2D square lattice (Ref.10).
4. because the stripe phase is spatially inhomogeneous, it is not easy to define appropriate boundary conditions for the MC simulation. Uniform twists will produce frustration.

The present work has revealed the existence of a smectic-like phase. This raises the question of the nature of the transition between the stripe phase and the (P) phase (line LC) and also between the stripe phase and the commensurate phase (line AC); for instance, if the transition line LC is not KT-like, one also needs to understand the nature of the critical regime along CD: for $\eta \ll 0.5$ one recovers a KT-transition

so there has to be some cross-over. Work is in progress to clarify that issue.

V. CONCLUSION

Using analytical techniques (NSCHA, a variational approach well suited for non collinear structures) and Monte Carlo simulations, we have studied the commensurate-incommensurate transition of the two dimensional XY model on a triangular lattice. Our study shows that this transition only occurs at $T = 0$. At finite temperature, the incommensurate structure evolves into a stripe phase made up of domains of left- and right-handed spirals separated by walls. The domain walls consist of the collinear structure. The nature of the phase transitions between the stripe phase and the ordered phases or between the stripe phase and the paramagnetic phase is an open problem.

ACKNOWLEDGMENTS

Monte Carlo calculations were performed on a Cray C98 thanks to contrat 960162 from IDRIS.

REFERENCES

- ¹ D.R. Hofstadter, Phys. Rev. **B 14**, 2239 (1976).
- ² Y. Hasegawa, M. Kohmoto, G. Montambaux, Phys. Rev. **B 48**, 1119 (1993).
- ³ I.-J. Hwang, and D. Stroud, Phys. Rev. **B 54**, 14978 (1996).
- ⁴ H.T. Diep, Magnetic Systems with competing interactions, World Scientific (1994).
- ⁵ V. Kalmeyer, R.B. Laughlin, Phys. Rev. **B 39**, 11879 (1989).
- ⁶ Y-H. Li, S. Teitel, Phys. Rev. **B 47**, 359 (1993); T. Chen, and S. Teitel, Phys. Rev. Lett. **72**, 2085 (1994); M. Franz and S. Teitel, Phys. Rev. Lett. **73**, 480 (1994); T. Chen, and S. Teitel, Phys. Rev. Lett. **74**, 2792 (1995).
- ⁷ There is a vast literature on this problem; see for instance references quoted in the following three articles:
- ⁸ M. Benakli, H. Zheng, M. Gabay, Phys. Rev. **B 55**, 278 (1997).
- ⁹ J.V. José, and G. Ramirez-Santiago, Phys. Rev. Lett. **77**, 4849 (1996).
- ¹⁰ P. Olsson, Phys. Rev. Lett. **75**, 2758 (1995).
- ¹¹ B. Berge, H.T. Diep, A. Ghazali, and P. Lallemand, Phys. Rev. **B 34**, 3177 (1986).
- ¹² J.M. Kosterlitz, D.J. Thouless, J. Phys. **C 6**, 1181 (1973); J.V. José, L.P. Kadanoff, S. Kirkpatrick, D.R. Nelson, Phys. Rev. **B 16**, 1217 (1977).
- ¹³ W.-M. Zhang, W.M. Saslow, and M. Gabay, Phys. Rev. **B 43**, 11285 (1991).

¹⁴ W.-M. Zhang, W.M. Saslow, M. Gabay, and M. Benakli Phys. Rev. **B 48**, 10204 (1993).

¹⁵ H. Kawamura, Prog. Theor. Phys. Jpn. Suppl. **101**, 545 (1990).

¹⁶ W.M. Saslow, M. Gabay, and W.-M. Zhang, Phys. Rev. Lett. **24**, 3627 (1992).

¹⁷ M. Collins, and W.M. Saslow, Phys. Rev. **B 53**, 8533 (1996).

¹⁸ R.M. Hornreich, M. Luban and S. Strikman, Phys. Rev. Lett. **35**, 1678 (1975).

¹⁹ P. Azaria, B. Delamotte, F. Delduc, T. Jolicoeur, Nuclear Physics **B 408**, 485 (1993).

²⁰ W. Selke, in Phase transitions and Critical Phenomena, Domb and Lebowitz Vol.15, p.2, Academic Press (1992).

²¹ T.A. Kaplan, Phys. Rev. Lett. **44**, 760 (1980); T. Garel, S. Doniach, J. Phys **C 13**, L887 (1980).

²² P. Minnhagen, Rev. Mod. Phys. **59**, 1001 (1987).

²³ M. Gabay, T. Garel, J. Phys. (Paris) **46**, 5 (1985); Phys. Rev. **B 33**, 6281 (1986).

²⁴ A. Kashuba, Phys. Rev. Lett. **77**, 2554 (1996).

²⁵ A.R. Day, T.C. Lubensky, and A.J. McKane, Phys. Rev. **A 27**, 1461 (1983); see also D.R. Nelson in Phase transitions and Critical Phenomena, Domb and Lebowitz Vol.7, p.89 Academic Press (1983).

²⁶ K.H. Fischer, and J.A. Hertz, in Spin Glasses, Cambridge University Press (1991).

²⁷ M. den Nijs, in Phase transitions and Critical Phenomena, Domb and Lebowitz Vol.12, p.219, Academic Press (1988).

²⁸ P. Olsson, Phys. Rev. Lett. **73**, 3339 (1994).

²⁹ P. Olsson, Phys. Rev. **B 52**, 4511 (1995).

³⁰ M. Benakli, E. Granato, Phys. Rev. **B 55**, 8361 (1997).

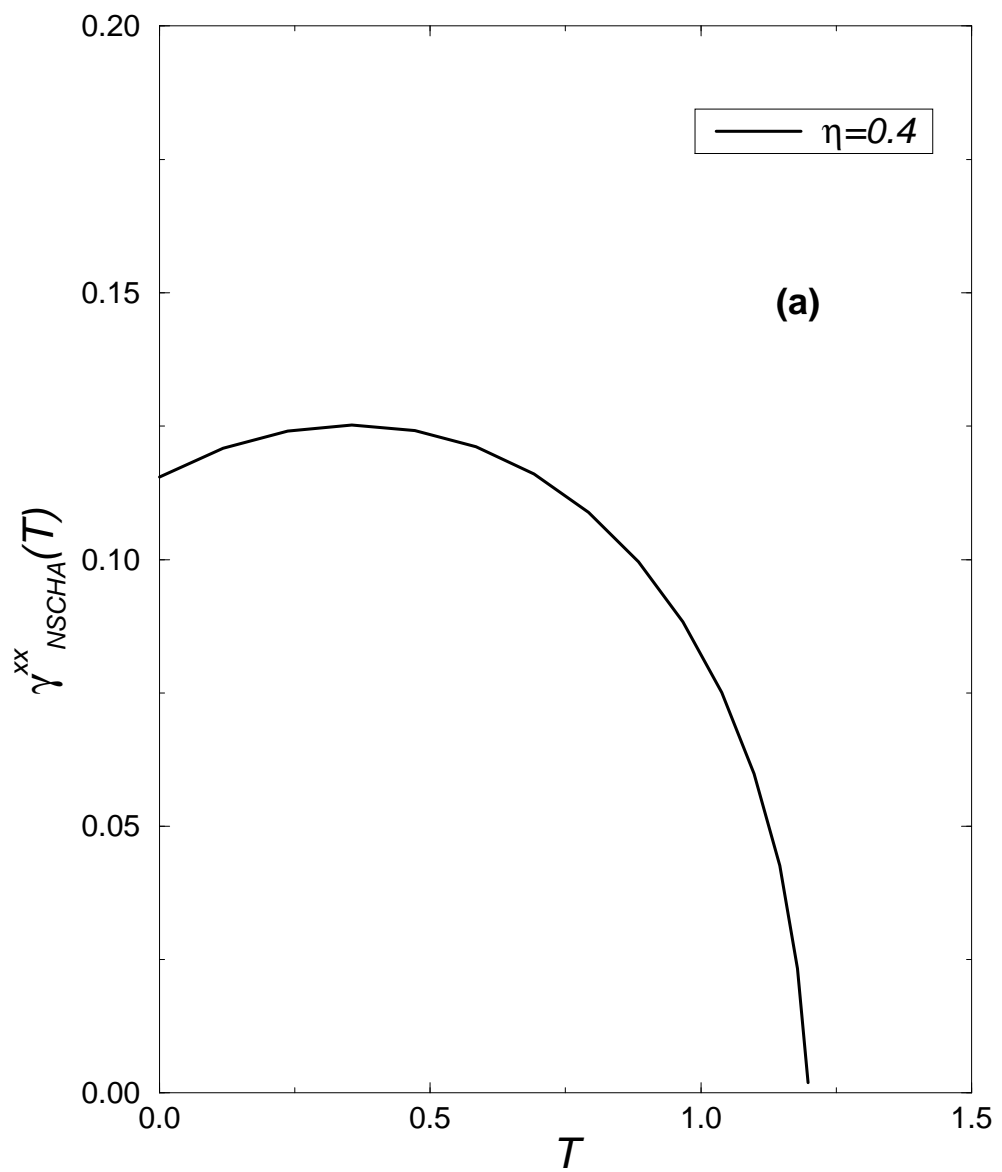
³¹ H. Eikmans, and J.E. van Himbergen, H.J.F. Knops, and J.M. Thijssen, Phys. Rev. **B 39**, 11759 (1989).

³² Eq.42 can be understood with the help of the following argument: using definition (39), the staggered chirality order parameter Σ (Eq.37) is expressed as a sum over nearest neighbor phase differences in the x direction. This sum is proportional to Q_x , so that χ_σ (Eq.40) contains the fluctuations of Q_x described by χ_{Q_x} . By Eq.35 one gets Eq.42

³³ G. Uimin and A. Pimpinelli, Phys. Rev. **E 49**, 1123 (1994).

³⁴ A. Pimpinelli, G. Uimin, and J. Villain, J. Phys. Condens. Matter **3**, 4693 (1991); J.L. Cardy, M.P.M. den Nijs, and M. Schick, Phys. Rev. **B 27**, 4251 (1983).

FIGURES



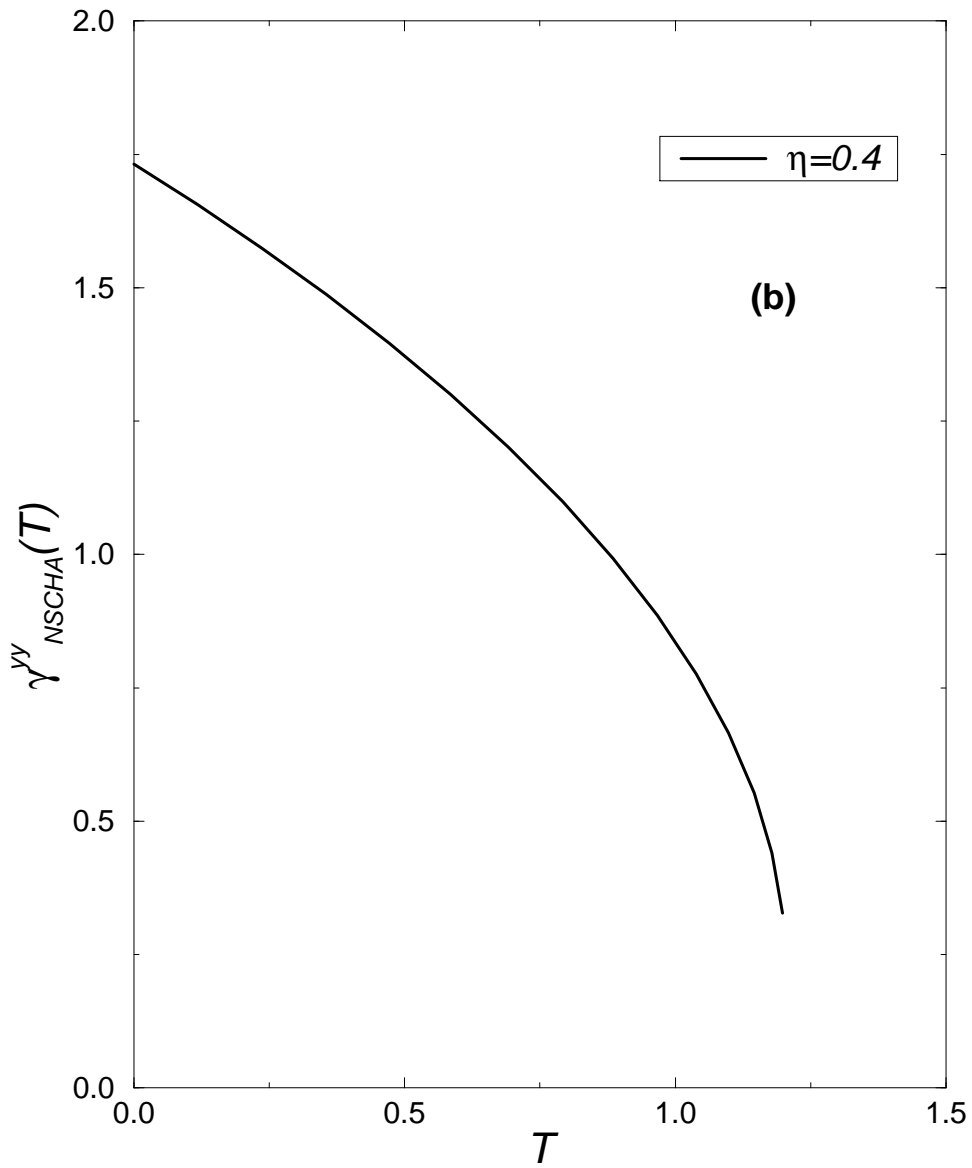


FIG. 1. NSCHA spinwave stiffnesses versus T for the row model, along the x direction (Fig 1a) and along the y direction (Fig 1b). Here $\eta = 0.40$ and the stiffnesses have been multiplied by a factor $\frac{2}{\sqrt{3}}$.

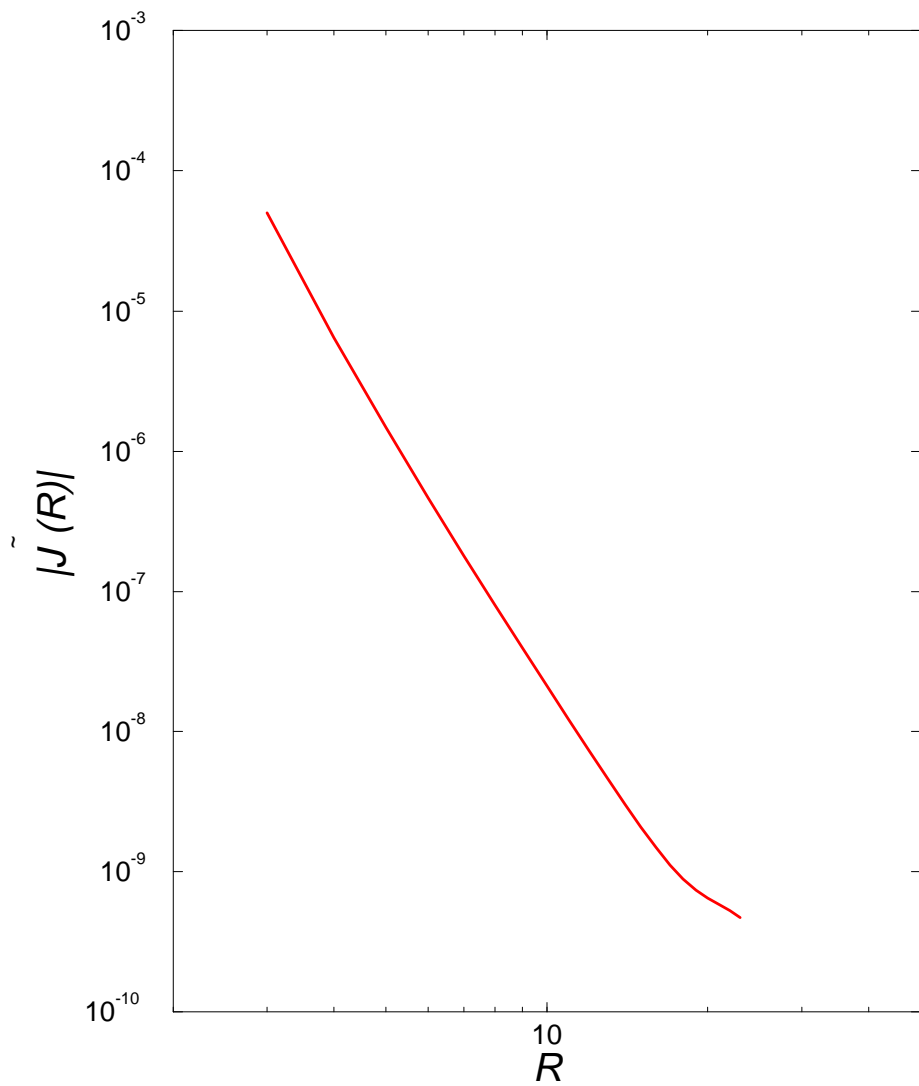


FIG. 2. $|\tilde{J}(R)|$ vs R for $T = 0.1J$ and $\eta = 0.575$. ($R = |\vec{r}_j - \vec{r}_i|$). The slope is 6 (see text).

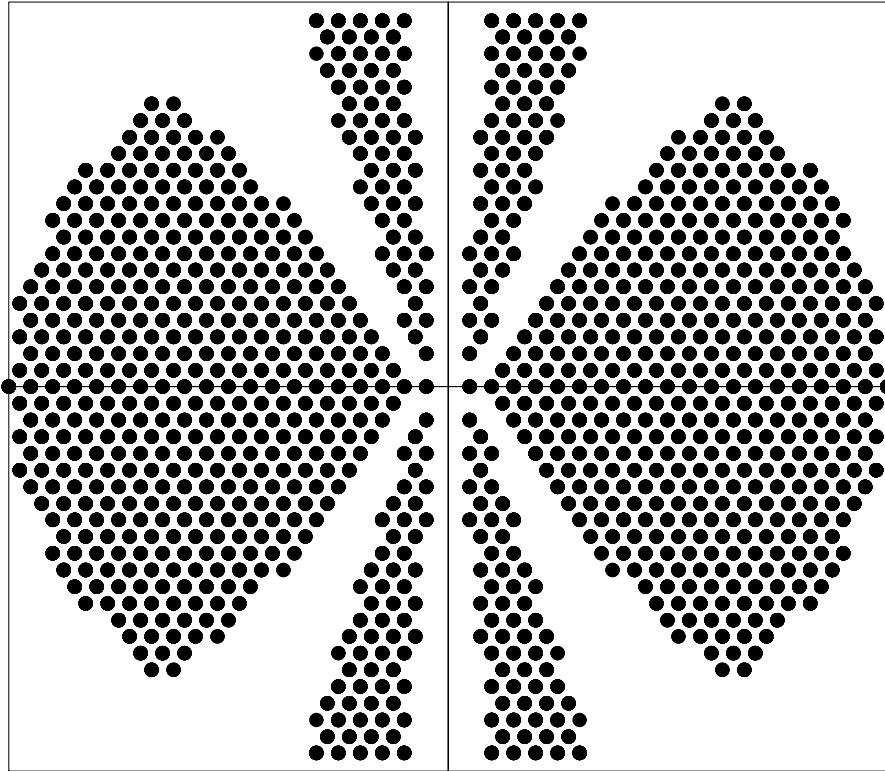


FIG. 3. The sign of \tilde{J}_{ij} at point \vec{r} for $\eta = 0.575$ and $T = 0.1J$. Circles denote sites where \tilde{J}_{ij} is negative. The horizontal axis corresponds to the direction of the η -bonds.

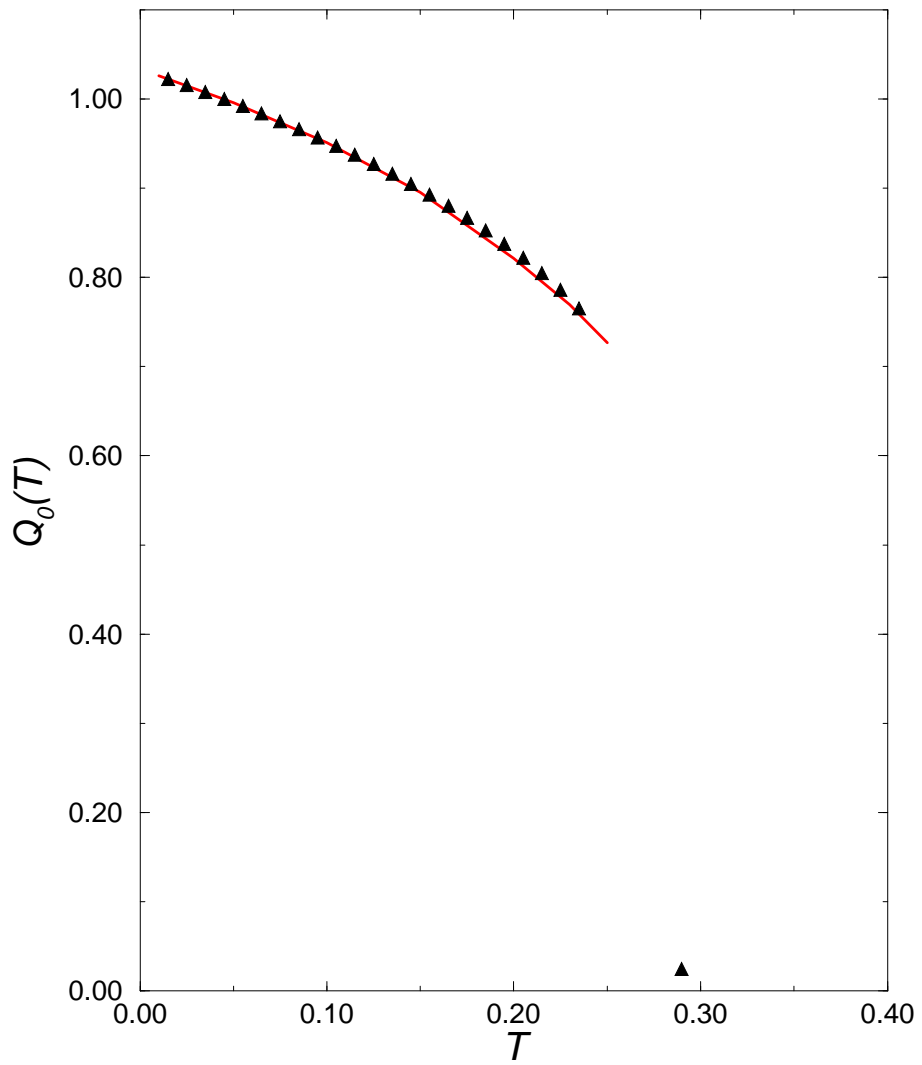
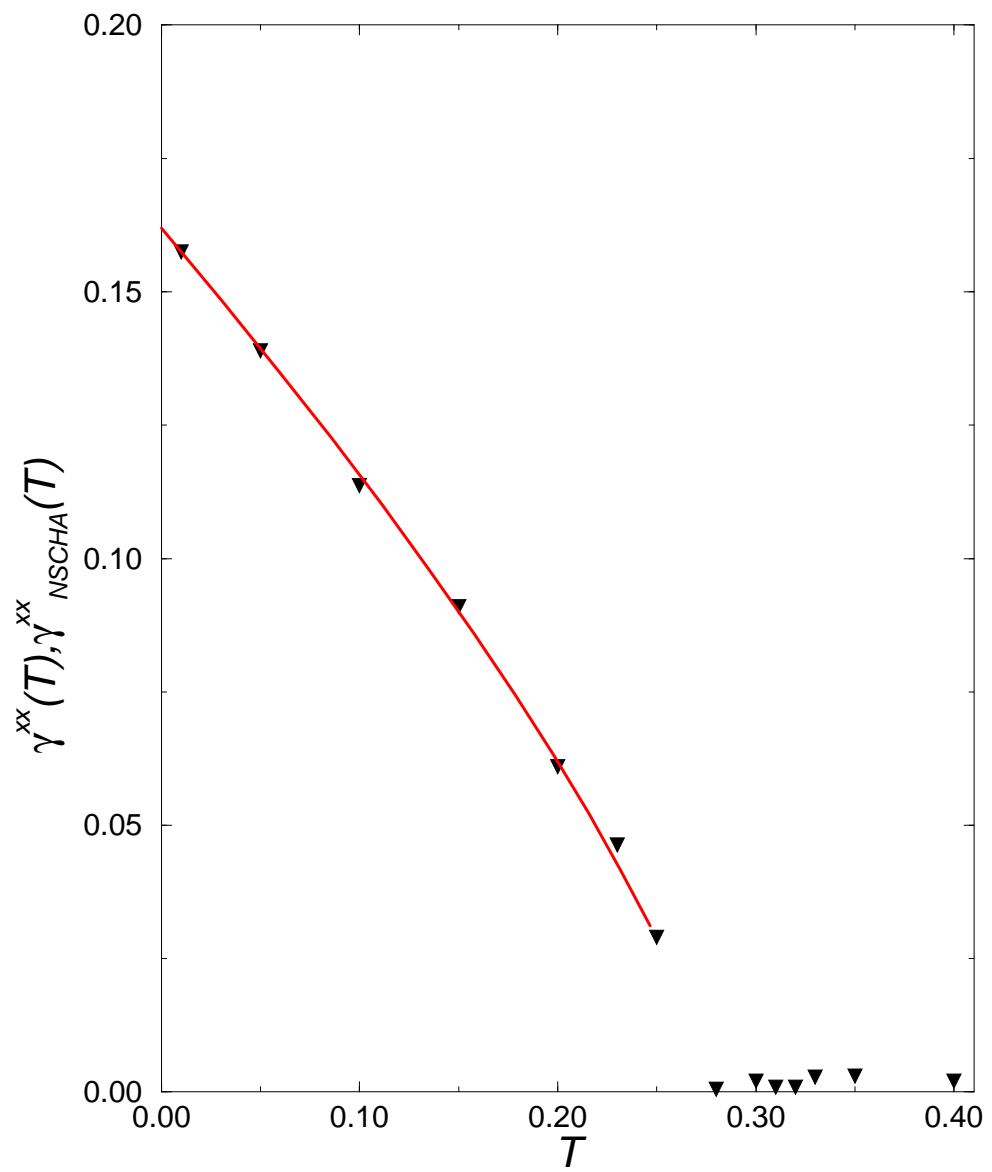


FIG. 4. $Q_0(T)$ vs T for $\eta = 0.575$. Triangles represent MC data for a 48^2 lattice and the solid line is the NSCHA prediction.



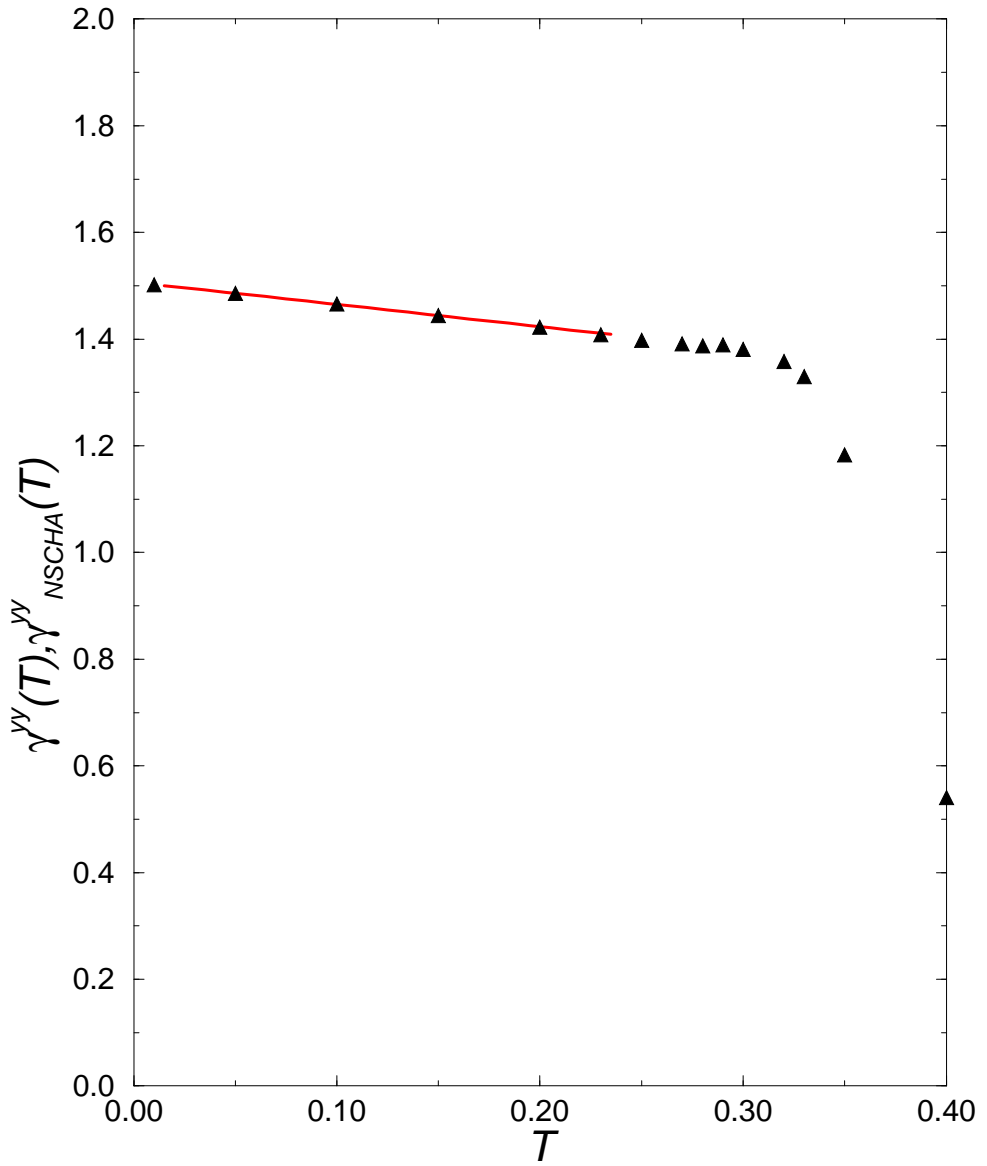


FIG. 5. Comparison of Monte Carlo and NSCHA stiffnesses in the x and y directions versus T for the row model when $\eta = 0.575$. Triangles represent MC data, solid line γ_{NSCHA} .

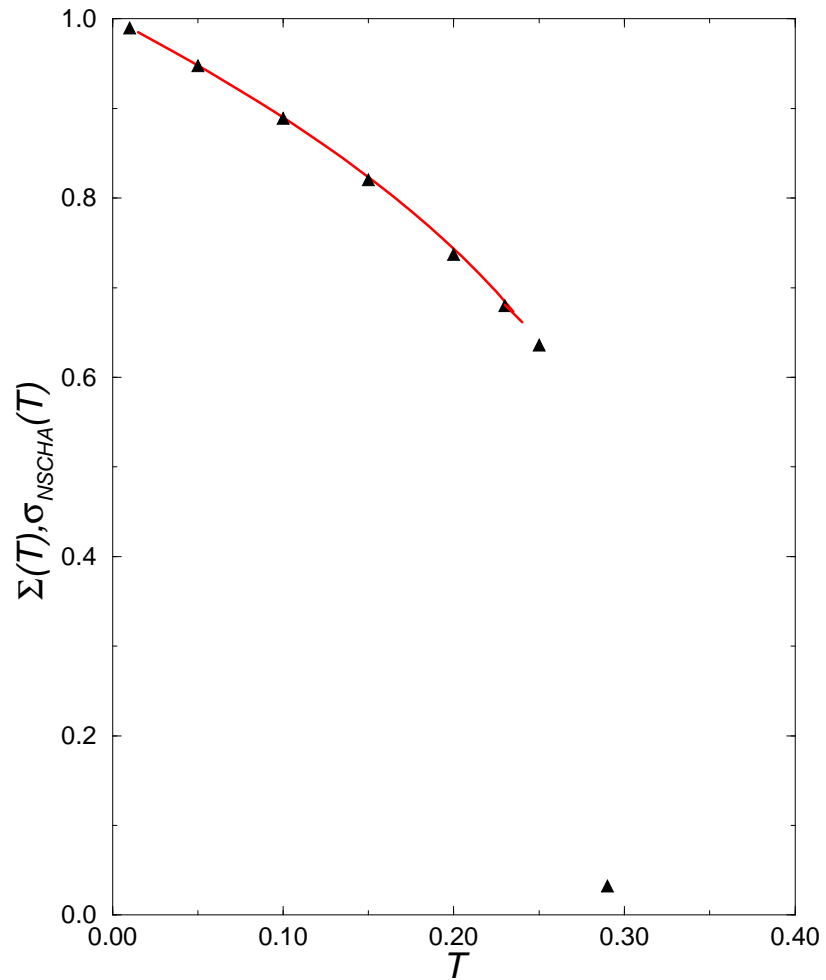


FIG. 6. Comparison of the Monte Carlo and NSCHA determined chiral order parameter. Triangles denote MC points for a 48^2 lattice Eq.37. Solid lines are the corresponding NSCHA predictions Eq.12.

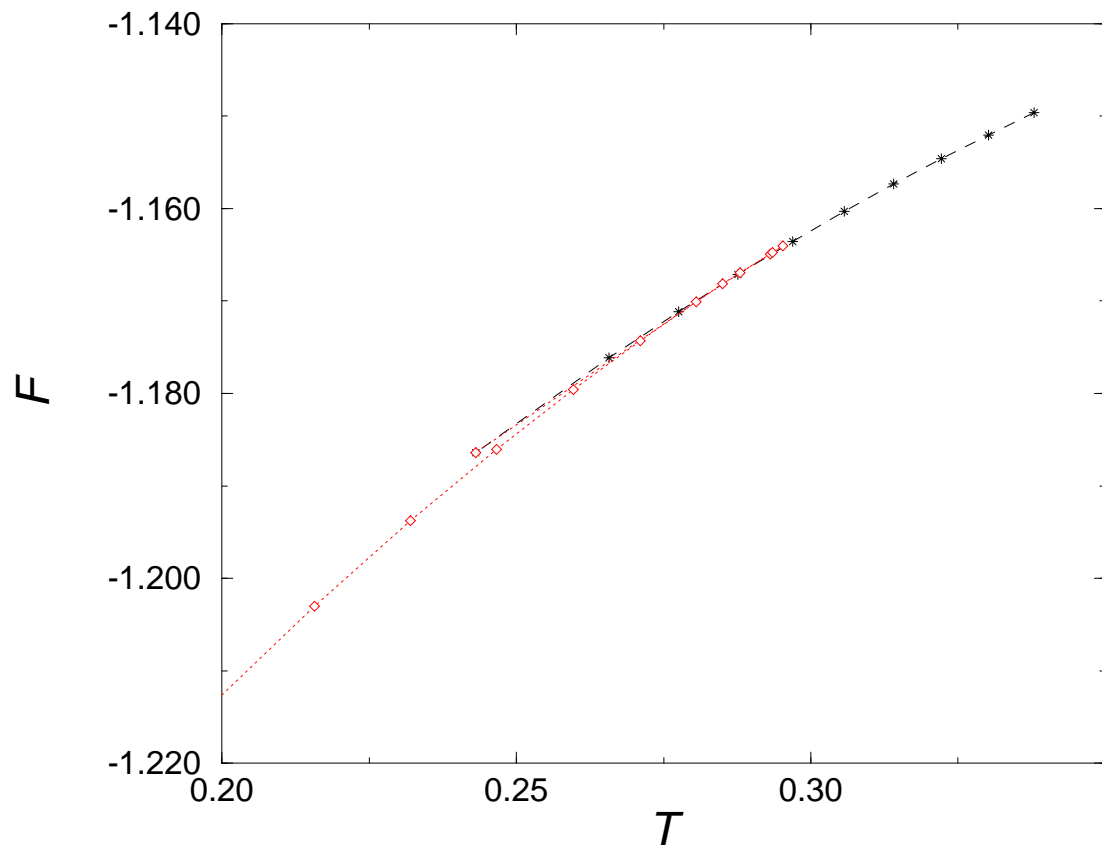


FIG. 7. NSCHA Free energy of the row model for $\eta = 0.575$ as a function of T , near the (C)-(IC) boundary. Open diamonds correspond to the spiral phase, stars correspond to the collinear phase. Dashed and dotted lines are guides for the eyes.

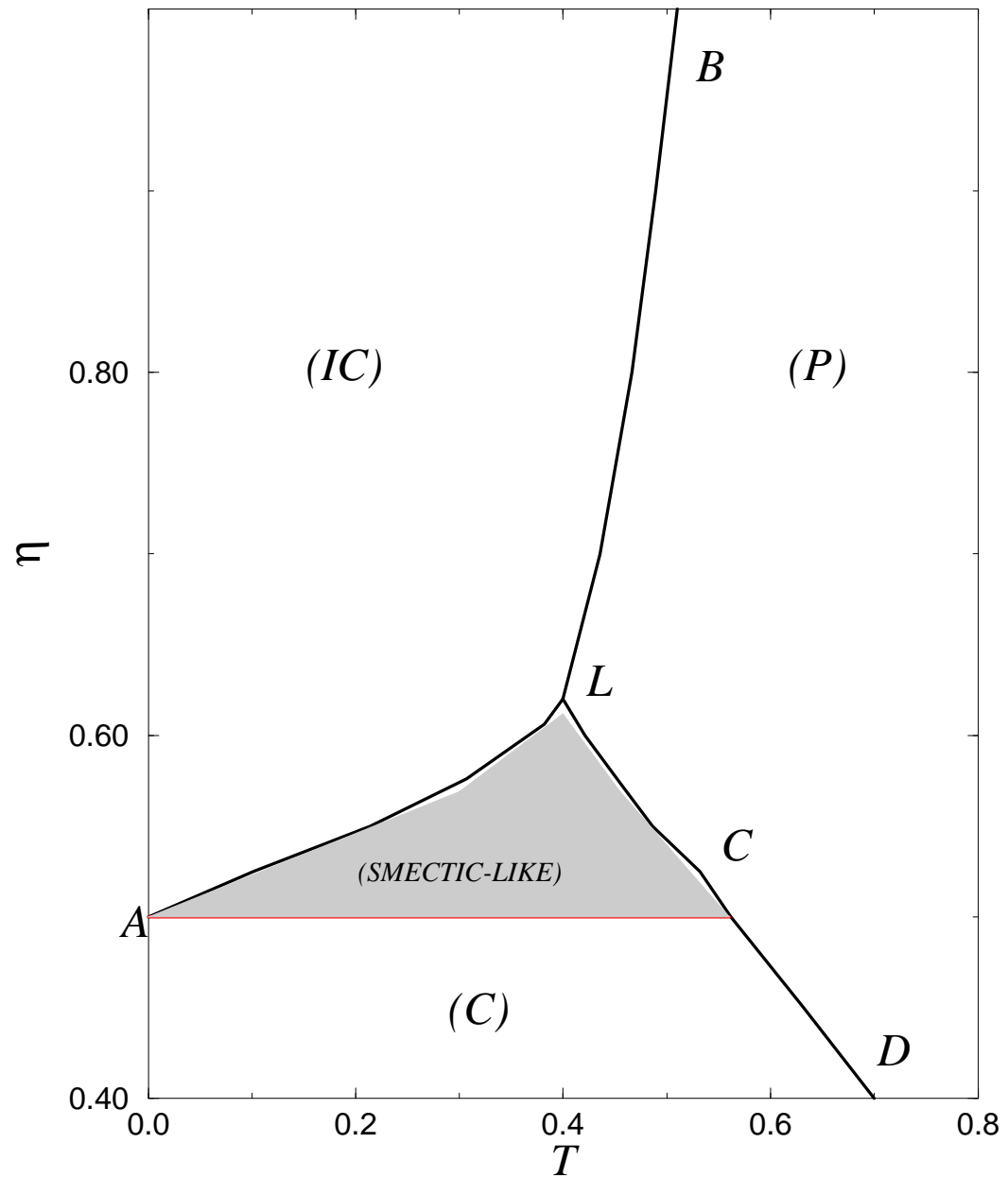


FIG. 8. MC phase diagram for the row model, in the (η, T) plane.

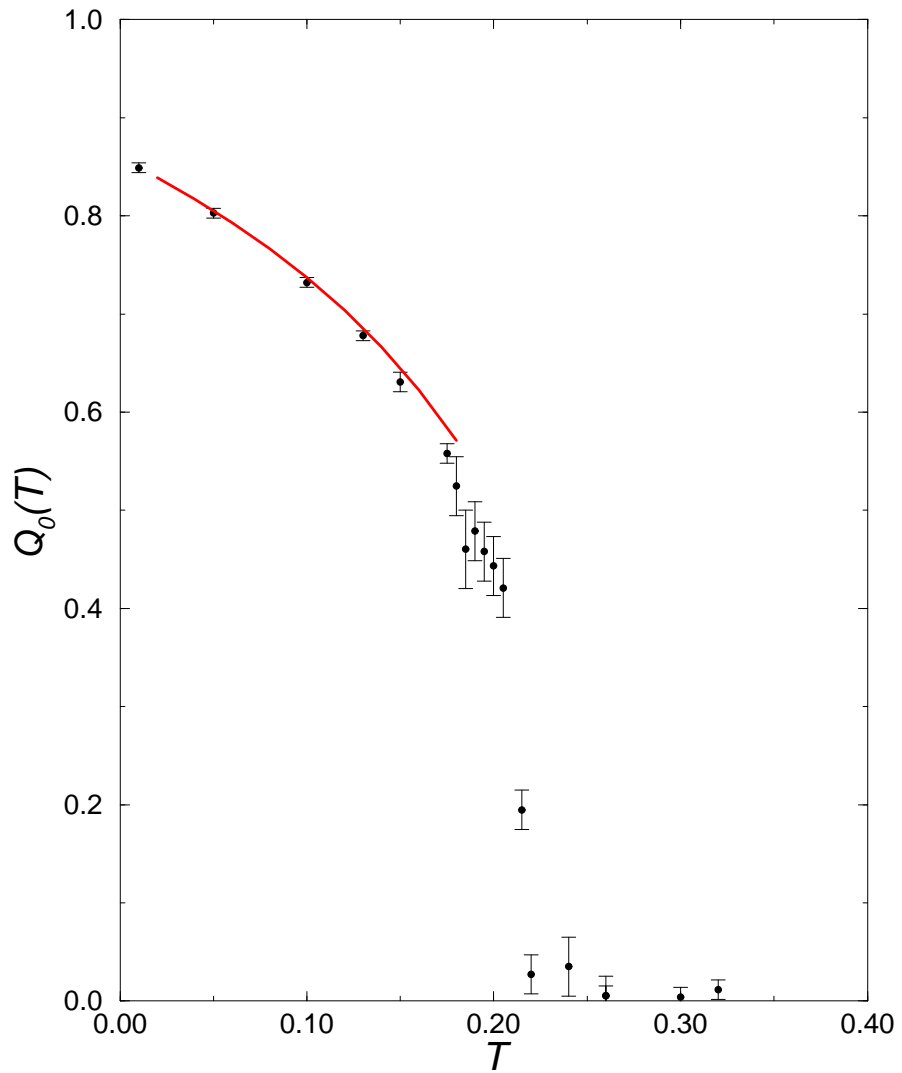


FIG. 9. $Q_0(T)$ versus T for $\eta = 0.55$. Filled circles represent MC data and the solid line is the NSCHA prediction.

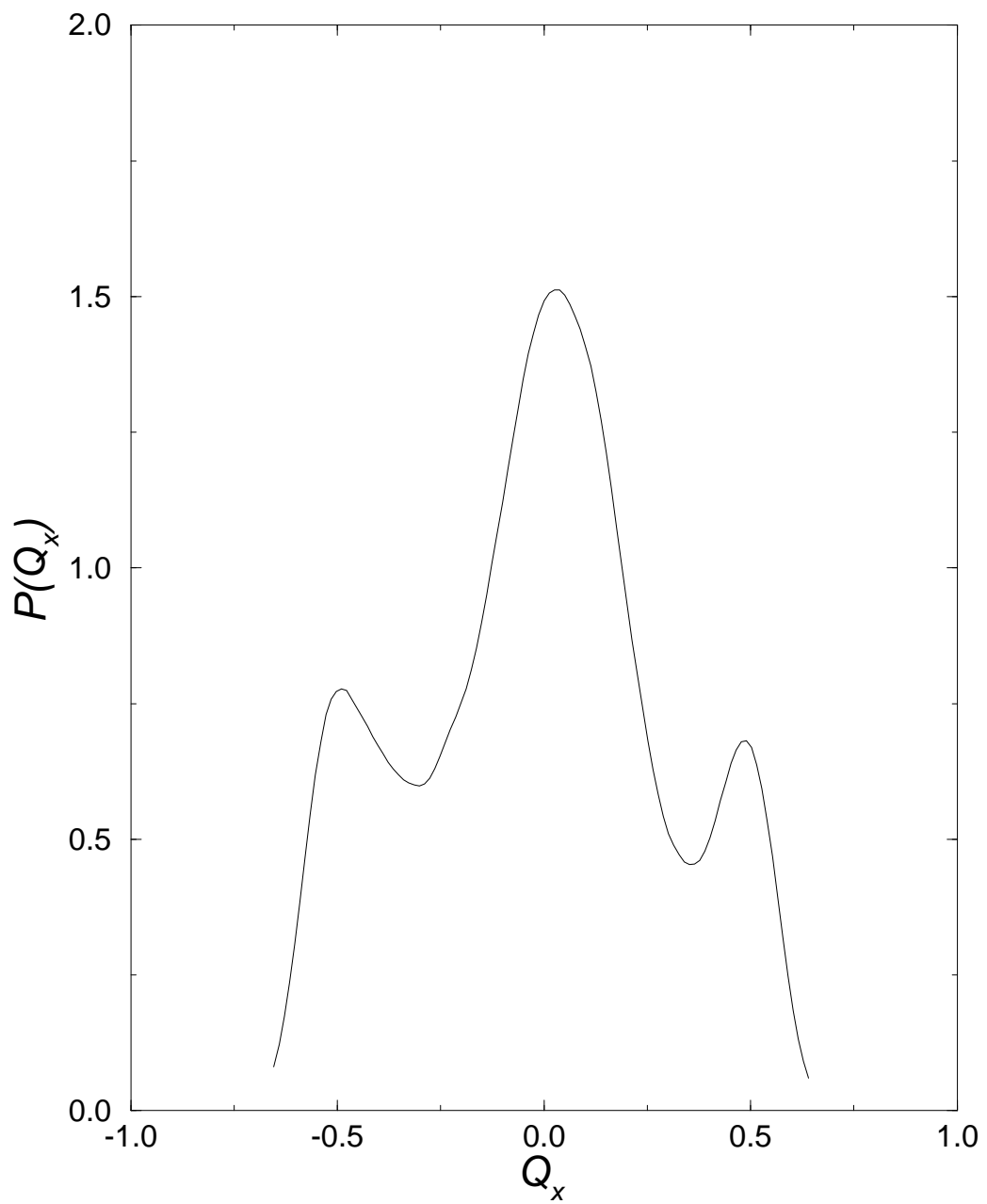


FIG. 10. $P(Q_x)$ versus Q_x for $\eta = 0.55$ and $T = 0.19J$.

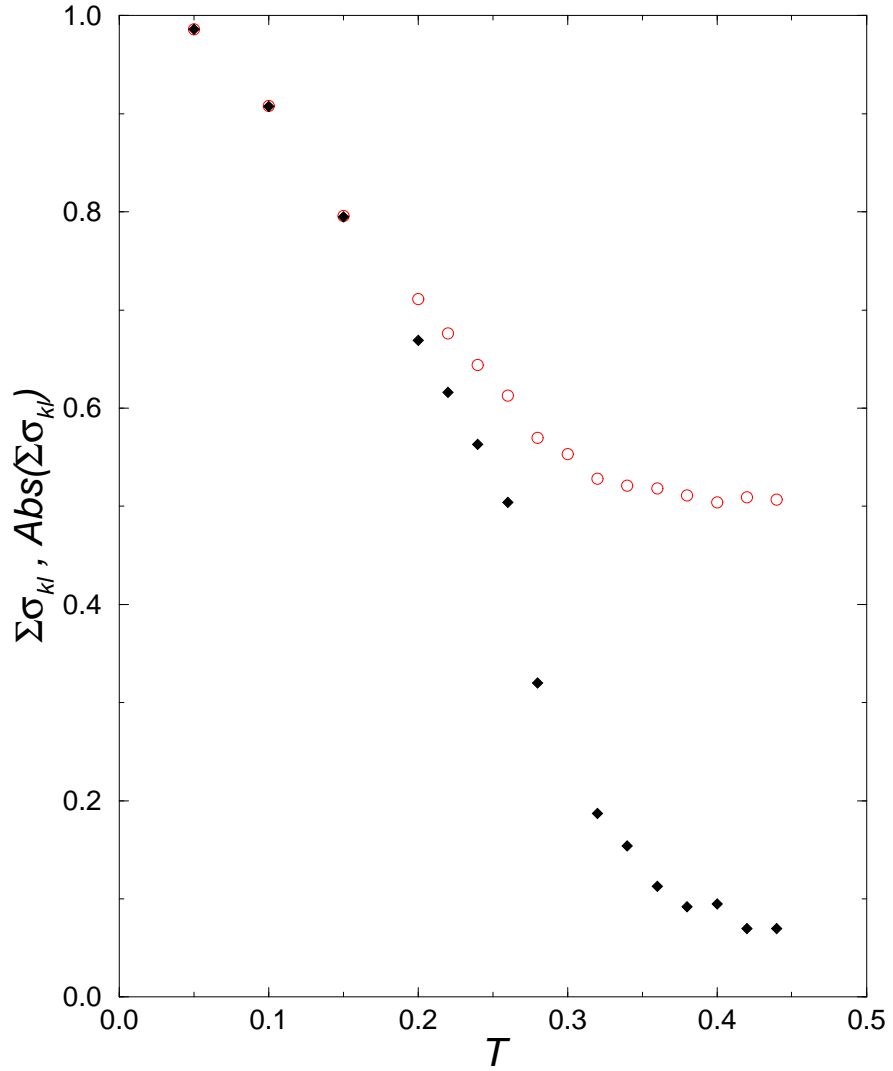


FIG. 11. MC determination of the plaquette chirality $\sum_{\langle kl \rangle \in P} \sigma_{kl}$ (filled diamonds) and of the absolute value of the plaquette chirality $\text{Abs}(\sum_{\langle kl \rangle \in P} \sigma_{kl})$ (open circles) versus T for $\eta = 0.575$.

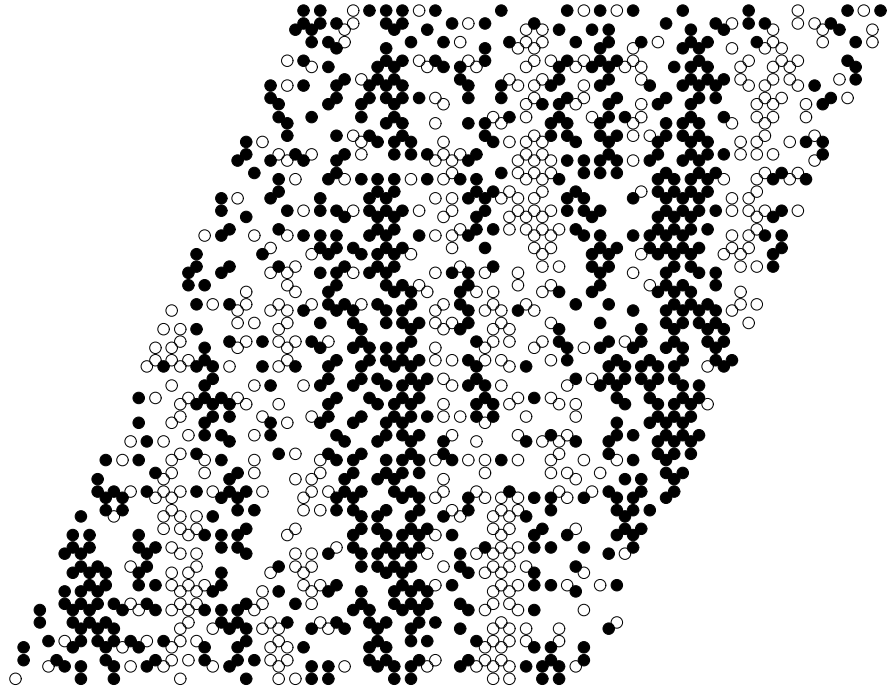
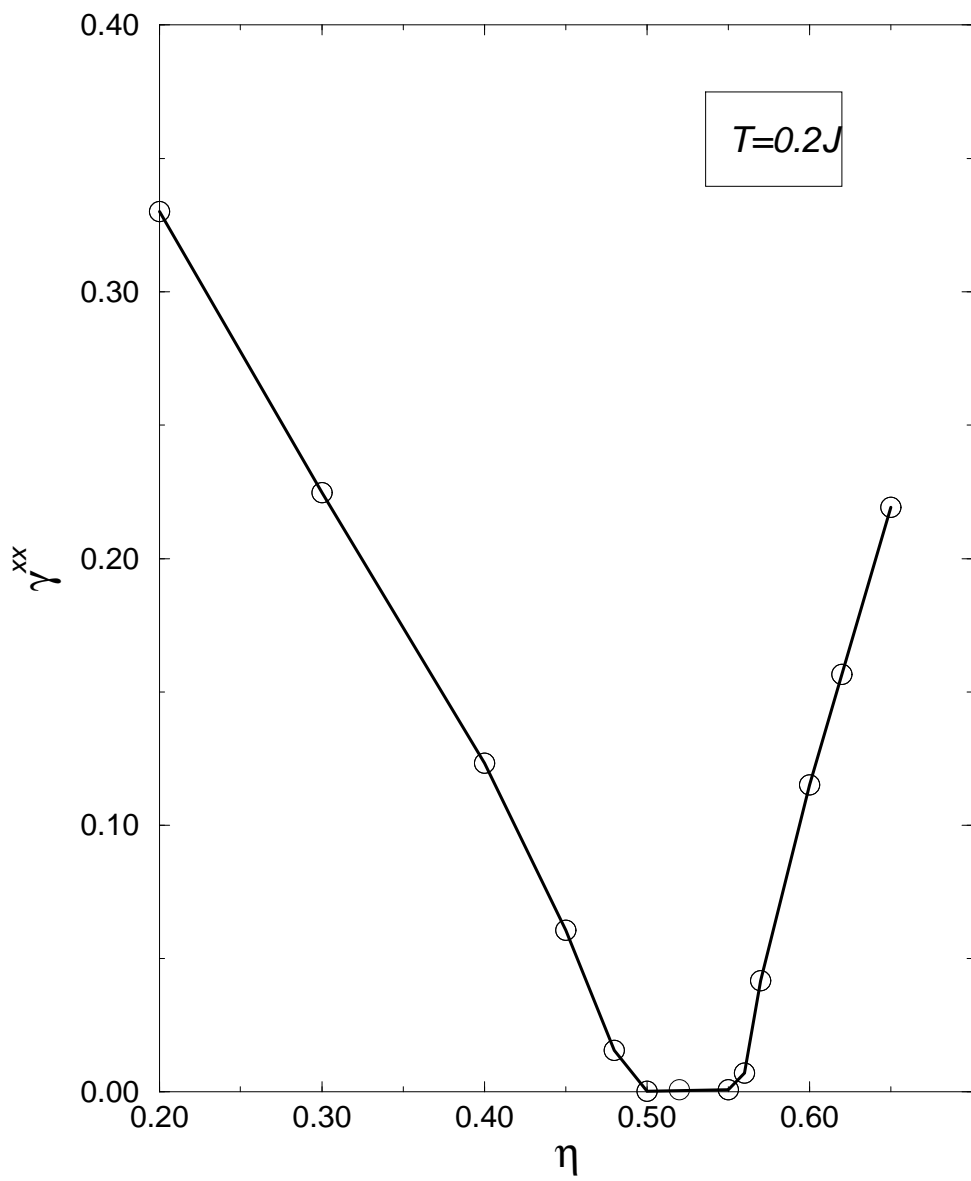


FIG. 12. Snapshot of chiralities on each plaquette of a 36^2 triangular lattice. $\eta = 0.575$ and $T = 0.4$. Filled circles represent plaquettes with the correct sign, i.e. in the same chiral state as at $T = 0$. Open circles correspond to plaquettes with the wrong sign, that is such that the chirality has changed compared to $T = 0$. Plaquettes with zero chirality (no symbol) are obtained in-between the two. One clearly sees a stripe structure of filled circles and open circles separated by domain walls of zero chirality.



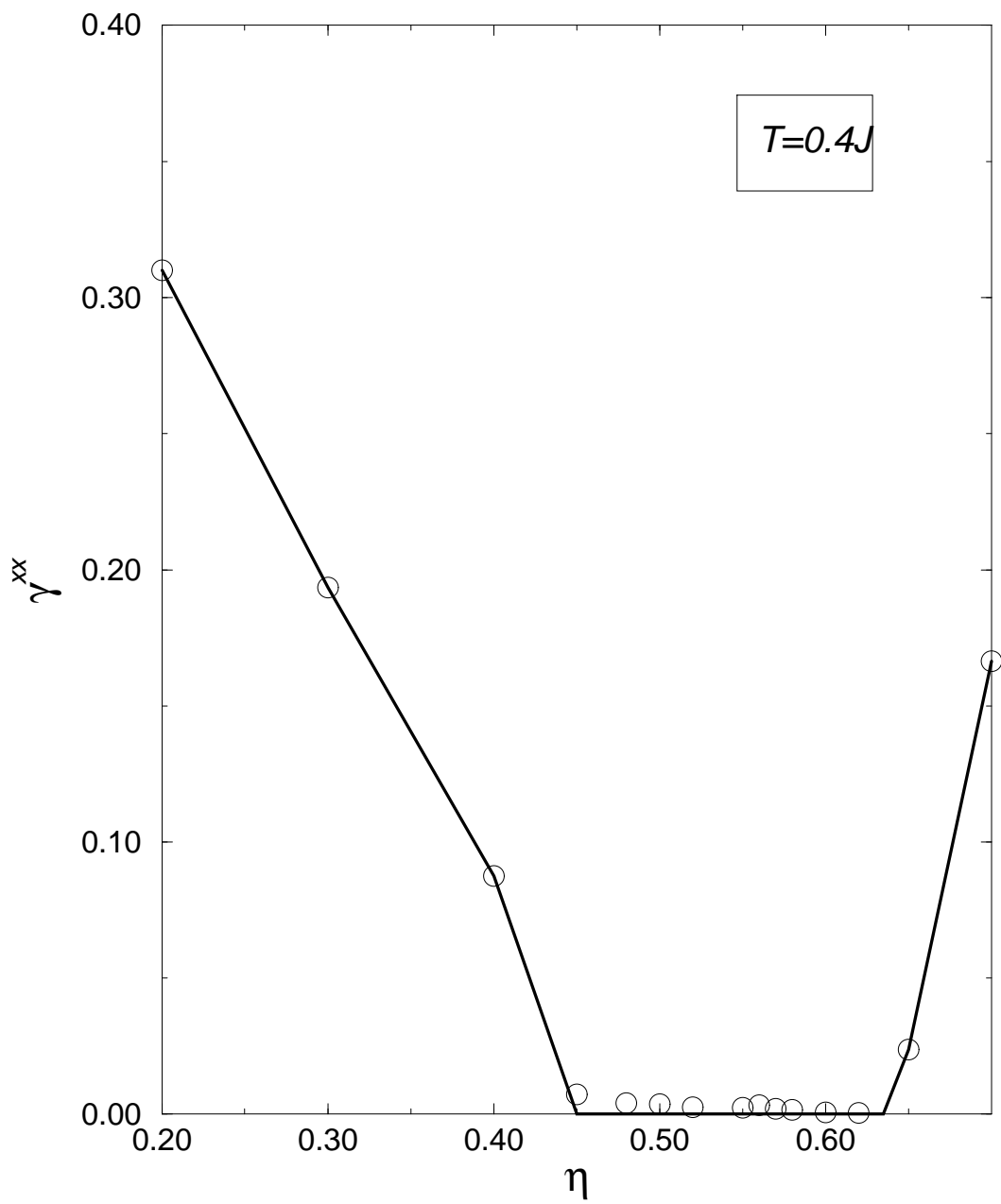


FIG. 13. MC data for γ^{xx} at fixed T , versus η . The lattice size is 48^2 . γ^{xx} is obtained from the histogram in Δ modulo $\frac{2\pi}{L}$. The region where $\gamma^{xx} = 0$ corresponds to the domain of stability of the stripe phase.

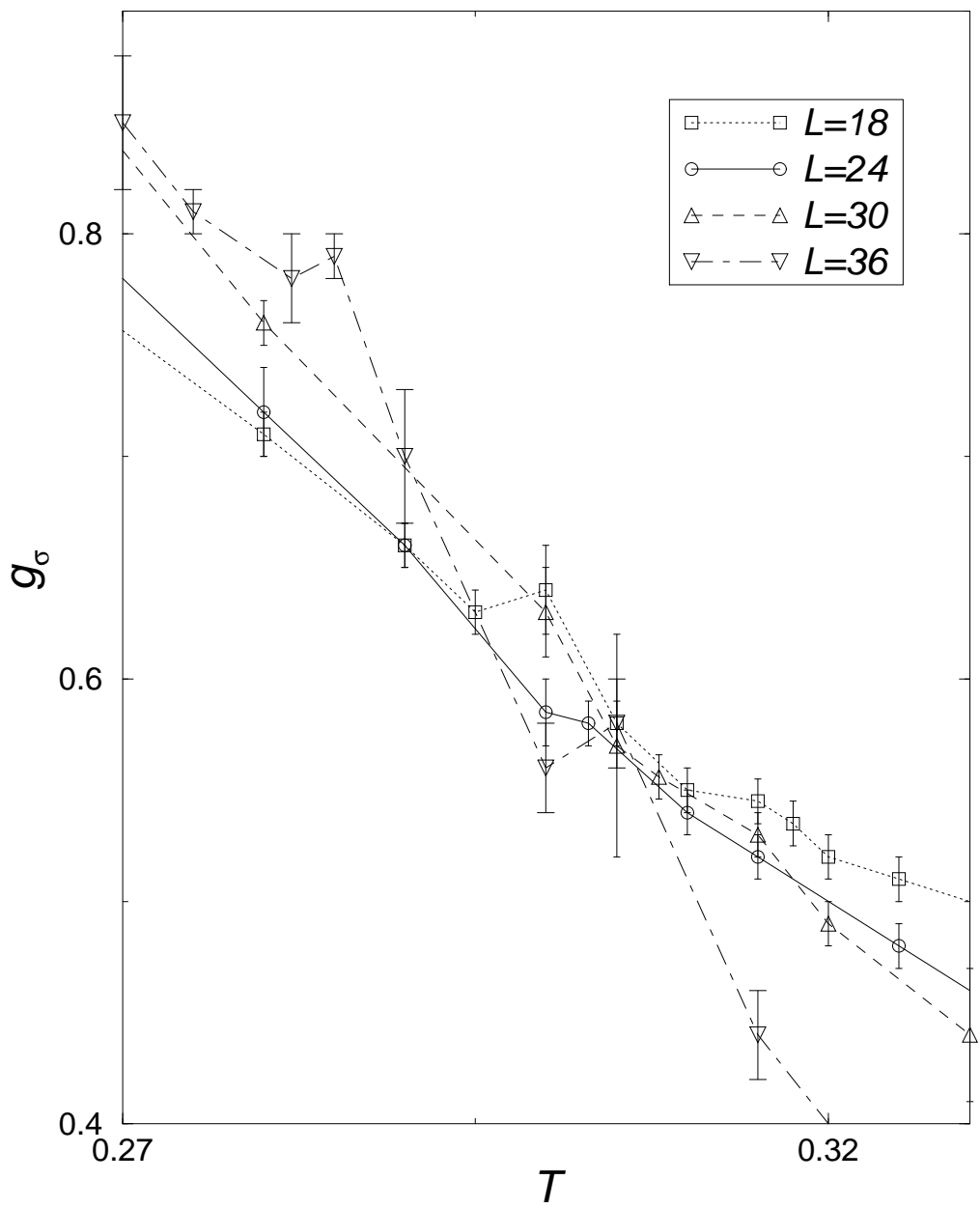


FIG. 14. Binder order parameter g_σ versus T for various sizes (Eq.41).